IEEE Access
Multidisciplinary ⋮ Rapid Review ⋮ Open Access Journal

Received January 30, 2022, accepted March 11, 2022, date of publication March 17, 2022, date of current version March 25, 2022.

Digital Object Identifier 10.1109/ACCESS.2022.3160544

3D Printing-Assisted Soft Capacitive Inclinometers for Simultaneous Monitoring of Tilt Angles and Directions

KEUNTAE BAEK[1], JOOHYUNG BANG[1], JIHUN LEE[1], MINYOUNG CHOI[1], AND HONGYUN SO[1,2], (Member, IEEE)

[1]Department of Mechanical Engineering, Hanyang University, Seoul 04763, South Korea
[2]Institute of Nano Science and Technology, Hanyang University, Seoul 04763, South Korea

Corresponding author: Hongyun So (hyso@hanyang.ac.kr)

This work was supported by the National Research Foundation of Korea (NRF) by the Ministry of Science and ICT of the Republic of Korea under Grant NRF-2020R1A4A1019074.

ABSTRACT This study presents capacitive-type inclinometers composed of flexible polymer pillars and dome-shaped roof frames that were manufactured using the three-dimensional (3D) printing method. Polylactic acid (PLA) filaments and acrylonitrile butadiene styrene (ABS) filaments were printed by the fused deposition modeling type 3D printer to fabricate the dome-shaped roof frames and the polymer curing molds, respectively. The operating principle of the inclinometer was to detect the change in capacitance between the helix-shaped electrode coiled around the polymer pillar and the built-in electrode in the roof frame. When the inclinometer was tilted, the polymer pillar was bent, and the physical distance between each electrode was changed with respect to the tilt angle and direction. Therefore, the tilt angles and directions were simultaneously estimated by distinguishing the capacitance and peak capacitance, respectively. The results of the experiments revealed that the inclinometer using the polymer pillar that was electrically connected to a standard weight and the roof frame with a roof angle of 45° exhibited a higher sensitivity (1.391 pF at a tilt angle of 40°) compared to those using roof angles of 90° and 135°. This study supports the use of 3D printing technology for the facile manufacturing of inclinometers that can detect tilt angles and directions simultaneously, which is not achievable with conventional inclinometers.

INDEX TERMS 3D printing, inclinometer, capacitive, polymer, rapid prototyping.

I. INTRODUCTION

Most vessels have a risk of overturning when they are inclined more than 45° to the left or right [1]. To address this problem, an inclinometer can be used for measuring the inclination angle of the tilted vessel [1]. In general, the inclinometers used in ships can be classified into analog and digital types. Although the analog-type inclinometer has the advantage of low cost, it cannot easily collect precise data and simultaneously measure the direction and angle [2], [3]. Although digital-type inclinometers have the advantage of measuring the direction and angle simultaneously, most of them involve expensive and complicated fabrication processes based on micro-electro-mechanical systems (MEMS) technology [4]–[13].

The associate editor coordinating the review of this manuscript and approving it for publication was Xiaokang Yin.

Most recent studies on inclinometers have focused on liquid-type inclinometers that use liquids, liquid metals, or electrolytes; however, such devices have a leakage risk [5]–[7], [11]–[17]. When liquid leaks, the device can lose its function as a sensor and yield an abnormal reading [1]. In particular, liquid metals are harmful to the human body and can induce severe health problems [18]–[20]. To prevent this, a complete sealing process and breakage prevention are needed, which require complex and additional manufacturing processes [5]–[7], [11], [14]. This problem can be mitigated by replacing the liquid with a solid as a working material. However, this method also has a complicated manufacturing process and generates a device with poor durability owing to the fatigue wear of solid materials during repeated measurements [2]–[4], [21].

Commercial inclinometers typically use a triaxial accelerometer or triaxial gyro sensor [8]–[10], [22]–[27].

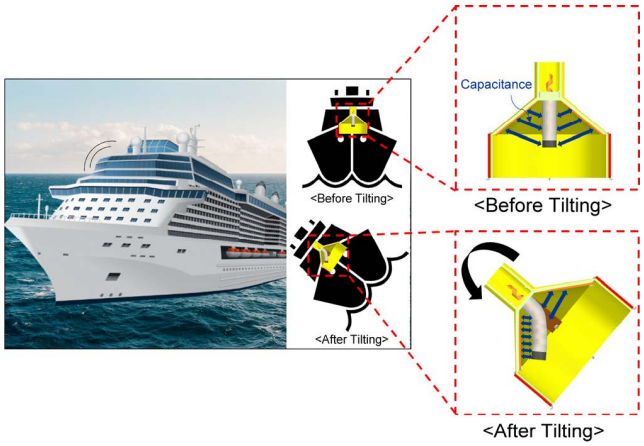

FIGURE 1. Schematic concept of the SCI combined with the 3D-printed PLA frame and the flexible polymer pillar to measure the capacitance with respect to the inclination angle.

Inclinometers using an accelerometer and gyro sensor must be calibrated as accurately as possible with changes in temperature, gain factors, and biases [24]–[27]. In addition, a complex algorithm and calibration are essential for measuring the inclination angle with such inclinometers. Some inclinometers have a large sensor drift, even with a small bias caused by external influences [27]. In particular, in an environment with many intense and repetitive movements (e.g., rolling, yawing, and pitching), such as the ocean, the inclinometer is subjected to mechanically harsh conditions and can exhibit abnormal measured values owing to sensor drift and offset [25]–[27]. Therefore, it is necessary to rapidly reset the device with an initial value once conditions permit [24], [25]. The measurement methods used in accelerometer-based inclinometers utilize piezoresistive [8], [10], [28], fiber optical [29]–[32], capacitive [8], [21], [23], [33], [34], resonant [35]–[38], and thermal properties [39]. Although most of the inclinometers that utilize these methods are significantly affected by external factors, such as temperature, in measuring values [25]–[27], the capacitive-type inclinometers are relatively less affected by changes in temperature than the piezoresistive-type inclinometers [10].

Recently, fused deposition modeling (FDM) three-dimensional (3D) printing has emerged as a rapid fabrication method for desired structures at low cost [40], [41]. In this study, a soft capacitive inclinometer (SCI) was fabricated and demonstrated using 3D printing methods, which allow for various filament selections and rapid fabrication. Figure 1 shows a schematic of the operating principles of the SCI, which uses the capacitance to measure the inclination angle and the tilt direction simultaneously. The SCI is composed of two parts: a 3D-printed polylactic acid (PLA) frame (roof) and a soft moving part with a flexible polymer pillar. Ecoflex, which was used for the polymer pillar, has the advantages of flexibility and rigidity when fully hardened [42]–[45]. Owing to their mechanical characteristics, Ecoflex polymers can address the low durability of solid-type inclinometers, which is a chronic problem caused by cracks or fatigue wear. For this reason, recently, polymer-based sensors have been widely used in various fields requiring durability and flexibility [46]–[49]. The SCI can simply measure the inclination angle and the tilt direction simultaneously and has a cost-effective and rapid fabrication method. The SCI has various applications in autonomous operations, such as those of autonomous drones, submarines, ships; civil

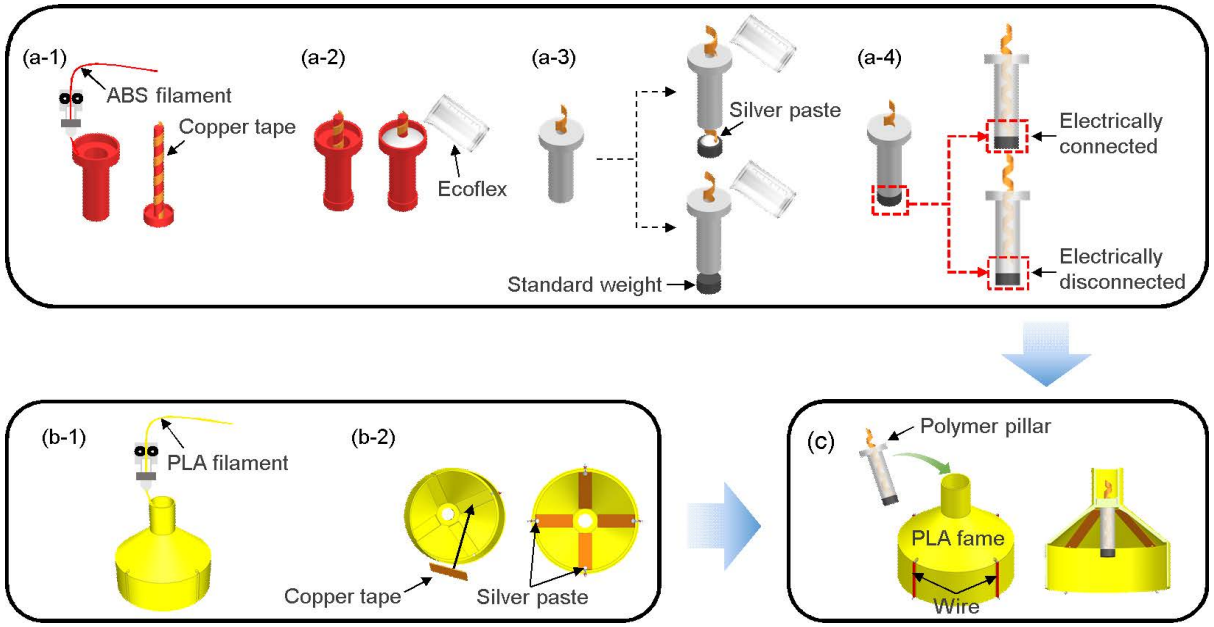

FIGURE 2. Overall fabrication process of the SCI. (a) Fabrication process of the Ecoflex-based polymer pillar: (a-1) printing of the ABS molds, (a-2) pouring and curing of the Ecoflex in the combined ABS molds, (a-3) separation of the Ecoflex pillar from the ABS molds and the manufacturing of two types of polymer pillars, and (a-4) filling the center cavity of the polymer pillar with Ecoflex and covering the standard weight with the polymer. (b) Fabrication process of the PLA-based roof frame: (b-1) printing of the PLA mold for the outer frame and (b-2) attaching the copper tapes (electrodes) in four directions and connecting with wires. (c) The final features of the SCI after combining the PLA roof frame and the polymer pillar.

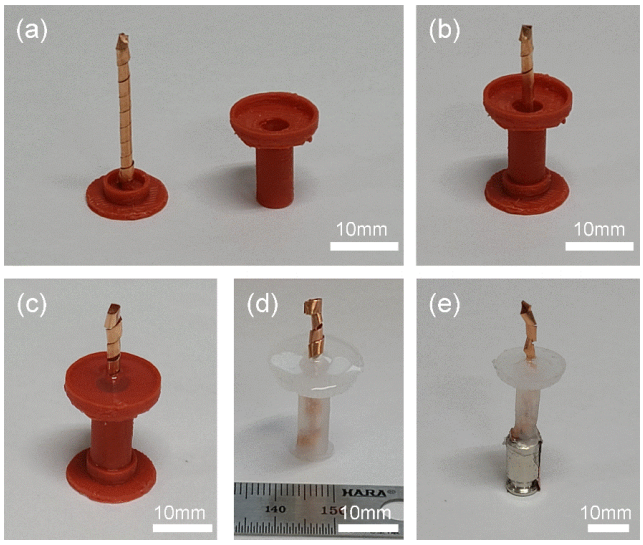

FIGURE 3. Optical picture of (a) printed ABS molds, (b) combined ABS molds, (c) poured elastomer in the combined ABS molds, (d) cured polymer pillar, and (e) polymer pillar combined with the standard weight.

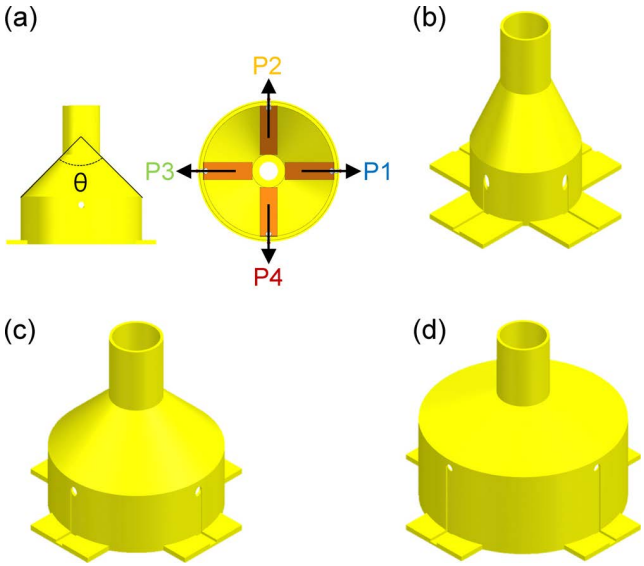

FIGURE 4. Images of the fabricated PLA roof frame (a) with various roof angles (θ): (b) $\theta = 45°$, (c) $\theta = 90°$, and (d) $\theta = 135°$.

engineering, such as in structural health monitoring; and in heavy industrial machinery, including excavators, cranes, and rotary drilling machines, which require position information about inclination to detect and prevent hazards.

II. EXPERIMENTAL METHODS

The SCI is composed of two main parts: a 3D-printed PLA frame with four electrodes and a flexible moving pillar that can be bent with respect to the inclination. Figure 2(a) shows the overall fabrication process of the polymer-based flexible pillar. The optical pictures of Fig. 2(a) were shown in Fig. 3. To create the polymer pillar, two types of molds were first printed using an FDM-type 3D printer (3DWOX 2X, Sindoh Co.) with an acrylonitrile butadiene styrene (ABS) filament (3DP200ARE-RQ, Ø1.75 mm, Sindoh Co.), as shown in Fig. 2(a-1). The 3D printing conditions used to fabricate two

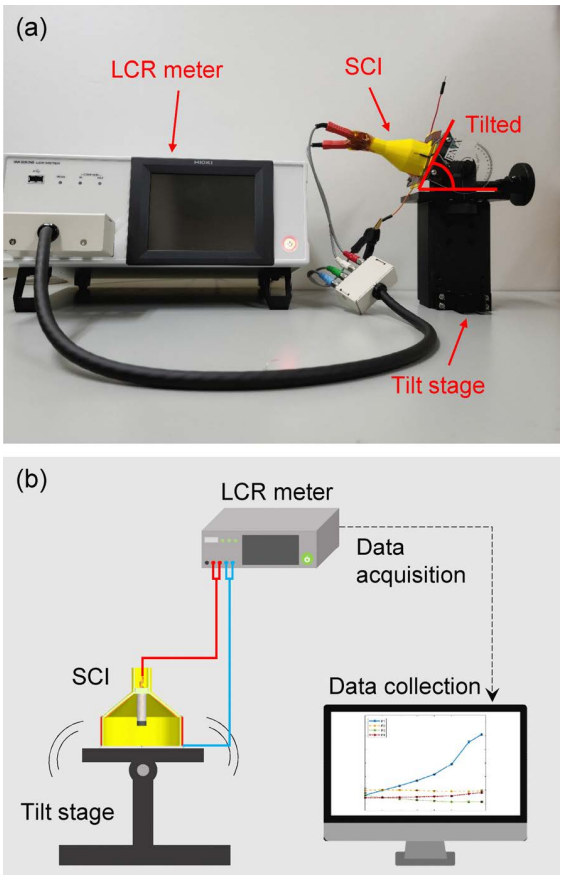

FIGURE 5. (a) Image of the experimental setup used to measure the inclination angle using the SCI. (b) Schematic of the experimental setup used to measure the inclination angle.

types of molds had a layer height of 0.2 mm, printing speed of 40 mm/s, extruder temperature of 230°C, stage temperature of 90°C, and nozzle diameter of 0.4 mm. The printed molds were composed of a hollow part and a cylindrical part. The copper tape was coiled around the cylindrical part in a helical shape, as shown in Fig. 3(a). Two parts of ABS molds were assembled, as shown in Fig. 3(b). The elastomer (Ecoflex 00-30, Smooth-on, United States) was then prepared by degassing and poured into the assembled ABS mold, as shown in Figs. 2(a-2) and 3(c). The Ecoflex was cured at room temperature for 4 h. The cured elastomer was then separated from the mold, as shown in Figs. 2(a-3) and 3(d). The adhesion force between ABS and the silicone elastomer is generally weak because both have low interfacial free energies [45]. Therefore, it was easy to separate the polymer pillar from the ABS mold. The separated elastomer had a cavity at the center, which was formed by the cylindrical part, and the cavity had a helix copper tape as an electrode. The cavity was filled again with Ecoflex and cured at room temperature for 4 h. To help the polymer pillar deform easily with variation in the inclination angle, we introduced a 5 g Ni-covered Fe standard weight (Kyeong-In Science Co.). In this study, two different types of polymer pillars were created to compare the device sensitivity: a pillar in which the standard weight and copper electrode were electrically connected and one in

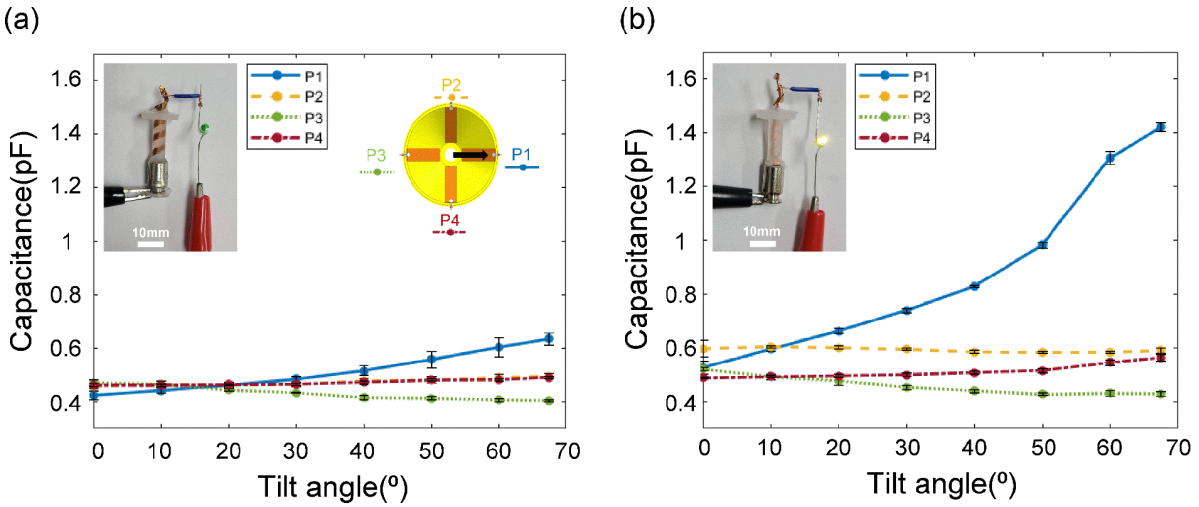

FIGURE 6. Sensing performance of the SCI with two types of polymer pillars: (a) a polymer pillar electrically disconnected from the standard weight and copper tape and (b) a polymer pillar electrically connected to the standard weight and copper tape. Inset images show the difference in electrical connection between two types of polymer pillars.

which the standard weight and copper electrode were not electrically connected. According to the non-parallel plate capacitance formula, the area and the capacitance of the electrodes are directly proportional. The capacitance of the SCI can be calculated using this non-parallel capacitance equation [50], as follows:

$$C = \int_0^l \frac{\epsilon_0 \epsilon_r w dy}{d\,(y)} = \frac{\epsilon_0 \epsilon_r w l}{d_2 - d_1} \ln\left(\frac{d_2}{d_1}\right) \quad (1)$$

where C, ϵ_0, ϵ_r, w, and l are the capacitance of the non-parallel plate, permittivity of the vacuum, dielectric constant, width of the electrode, length of the electrode, respectively. d_1 and d_2 are the short and long distances between two ends of the non-parallel electrodes, respectively. Thus, the SCI using the electrically connected pillar is expected to show higher capacitance due to the increased area of electrode compared to that using the electrically disconnected pillar. In the case of the electrically connected polymer pillar, the standard weight and copper tape were glued using silver paste (Fig. 3(e)), and the standard weight was covered again by a thin layer of elastomer to provide the same dielectric properties and prevent physical collisions between the electrodes in the PLA frame and the polymer pillar. In contrast, in the case of the electrically disconnected polymer pillar, the standard weight and copper tape were simply glued using the elastomer for electrical disconnection. Figure 2(a-4) shows a schematic of the fabricated polymer pillar. The total length of the polymer pillar and standard weight were 34 mm and 13 mm, respectively. The diameters of the lower and upper parts were 6 mm and 16 mm, respectively, whereas that of the standard weight was 8 mm. It should be noted that Ecoflex enables rapid deformation and recovery of the initial shape with less fatigue and cracking owing to its viscoelasticity [42]–[45].

To investigate the measurement range and device sensitivity with respect to the roof angle of the PLA frame, three different frames with roof angles (θ) of 45°, 90°, and 135° were prepared in this study, as shown in Fig. 4. Each frame was designed to have copper electrodes with the same area (Fig. 4(a)) but different roof angles of 45°, 90°, and 135°, as shown in Figs. 4(b), 4(c), and 4(d), respectively. Figure 2(b) shows the overall fabrication process of the roof frames. The roof frames were printed using an FDM-type 3D printer with a PLA filament (3DP200PYE-RQ, Ø1.75 mm, Sindoh Co.), as shown in Fig. 2(b-1). The 3D printing conditions used to fabricate the roof frames had a layer height of 0.2 mm, printing speed of 40 mm/s, extruder temperature of 200°C, stage temperature of 60°C, and nozzle diameter of 0.4 mm. The printed PLA frames were designed to attach four copper electrodes (10 mm × 28 mm) along four directions with 90° spacing (i.e., P1, P2, P3, and P4 directions), as shown in Fig. 4(a). The wires were then electrically connected to the copper electrodes using silver paste.

III. RESULTS AND DISCUSSION

Figure 5 shows the experimental setup for measuring the capacitance change between two electrodes within the roof frame and polymer pillar with respect to the tilt angle. The system consists of a tilt stage of a water contact angle goniometer (Phoenix-MT(A), Surface Electro Optics, Korea), the SCI, and an LCR meter (IM3536, HIOKI Corp.). The SCI is a combination of the polymer pillar and PLA roof frame, as shown in Fig. 2(c). The SCI was attached to the tilt stage using Kapton tape. Subsequently, wires from the LCR meter were connected to the polymer pillar and four wires on the roof frame to measure the capacitance in four directions. As shown in Fig. 5(a), the change in capacitance for various tilt angles was measured by tilting the tilt stage at 10° intervals from 0° to the maximum tilt angle of 67.5°. Different inclinations were controlled by manually turning the knob of the tilt stage. All the experiments were conducted by measuring the data for 10 s after a saturation time of 5 s. The experiments were conducted five times under the same conditions to demonstrate reliable operation, and the mean and standard deviation of the experimental values were

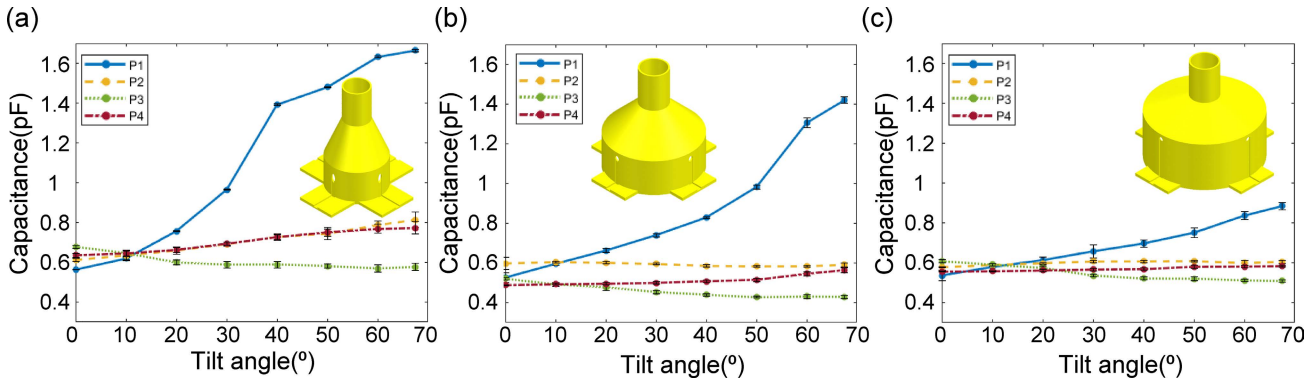

FIGURE 7. Sensing performance of the SCIs with three different roof frame angles: (a) 45°, (b) 90°, and (c) 135°.

obtained for each average capacitance value. The performances of the inclinometers were compared and analyzed by plotting the experimental values, as shown in Fig. 5(b).

To compare the performance of the two types of polymer pillars based on the electrical connection/disconnection between the helix copper electrode and the standard weight, experiments were conducted on two specimens on a PLA frame with a frame angle of 90°. Figure 6 shows the capacitance changes of the two types of SCIs. The two SCIs were tilted up to 67.5° in the P1 direction. In both types of SCIs, as the tilt angle increased in the P1 direction, the capacitance between the pillar and electrode in the P1 direction gradually increased because the distance between the two electrodes was closer than that of the electrodes in the other directions. In contrast, there was no significant capacitance change between the pillar and electrodes in the P2 and P4 directions; however, a reduction was observed in the P3 direction because the distance between the pillar and electrode increased in the P3 direction. For the maximum rate of capacitance change in the P1 direction, the polymer pillar, which was electrically disconnected from the standard weight, exhibited a 1.5 times larger capacitance when the SCI was tilted at 67.5° (i.e., from 0.424 pF to 0.635 pF, as shown in Fig. 6(a)). However, the SCI using the polymer pillar, which was electrically connected to the standard weight, exhibited a 2.7 times larger capacitance (i.e., from 0.526 pF to 1.419 pF) at the same tilt angle (i.e., 80% increase in sensitivity), as shown in Fig. 6(b). This might be because the polymer pillar with an electrical connection between the helix electrode and standard weight had a larger electrode surface area, thus increasing the overall capacitance between the pillar and roof frame electrodes. Therefore, the SCI using the polymer pillar in which the helix electrode was electrically connected to the standard weight was used for further experiments and analysis.

To characterize the sensing performance of the SCIs with respect to the roof frame angle, experiments were conducted using an electrically connected polymer pillar with PLA frames with roof angles of 45°, 90°, and 135°. Figure 7(a) shows the experimental results for a roof frame angle of 45°. In the tilt direction (P1), the capacitance increased significantly from 0.563 pF to 1.391 pF at a tilt angle of 40°. When the tilt angle exceeded 40°, the capacitance increased almost linearly. This might be because the standard weight of the polymer pillar made physical contact with the electrode surface in the roof frame at a tilt angle of 40°. Subsequently, the Ecoflex layer covering the standard weight was compressed as the tilt angle exceeded 40°; thus, the capacitance increased almost linearly. The capacitance change due to the compression of the Ecoflex coating layer changed the distance between the pillar electrode and electrode in the roof frame through different mechanisms, while the distance was only changed by the bending of the polymer pillar at a tilt angle lower than 40°. In the case of the SCIs with roof frame angles of 90° and 135°, the distance between the pillar electrode and electrode in the roof frame was only changed by the bending of the polymer pillar.

Figures 7(b) and 7(c) show the sensing performance of the SCIs with roof frame angles of 90° and 135°, respectively. A comparison of the performances of the SCIs with three different roof frame angles tilted in the P1 direction revealed that the change rate in capacitance of the SCI using the PLA frame with a roof angle of 45° (147.1% increase at a tilt angle of 40°) was greater than those of the SCIs with roof angles of 90° (57.4% increase at a tilt angle of 40°) and 135° (29.8% increase at a tilt angle of 40°). The average sensitivity of the SCI decreased as the roof angle increased. This might be because the distance between the pillar electrode and the electrode on the roof frame angled at 135° was not close enough for a large capacitance to be generated. This also indicates that the distance between the two electrodes is a key parameter in the design of capacitive-type inclinometers with high sensitivity. In this study, the SCI with a roof angle of 45° exhibited the most sensitive performance, and it enabled the distinct measurement of small inclinations, even those as small as 10° (Fig. 7(a)), which was not achieved using other SCIs (Figs. 7(b) and 7(c)).

To demonstrate that the SCI could distinguish the tilt direction as well as the tilt angle, the SCI using the roof frame angle of 45° was tilted at 40° in a total of eight directions (i.e., P1, P2, P3, P4, and four intermediate directions between them). The experiments were performed using three samples of the SCI under the same conditions, and the results exhibited small deviation between each sample, showing a good yield of

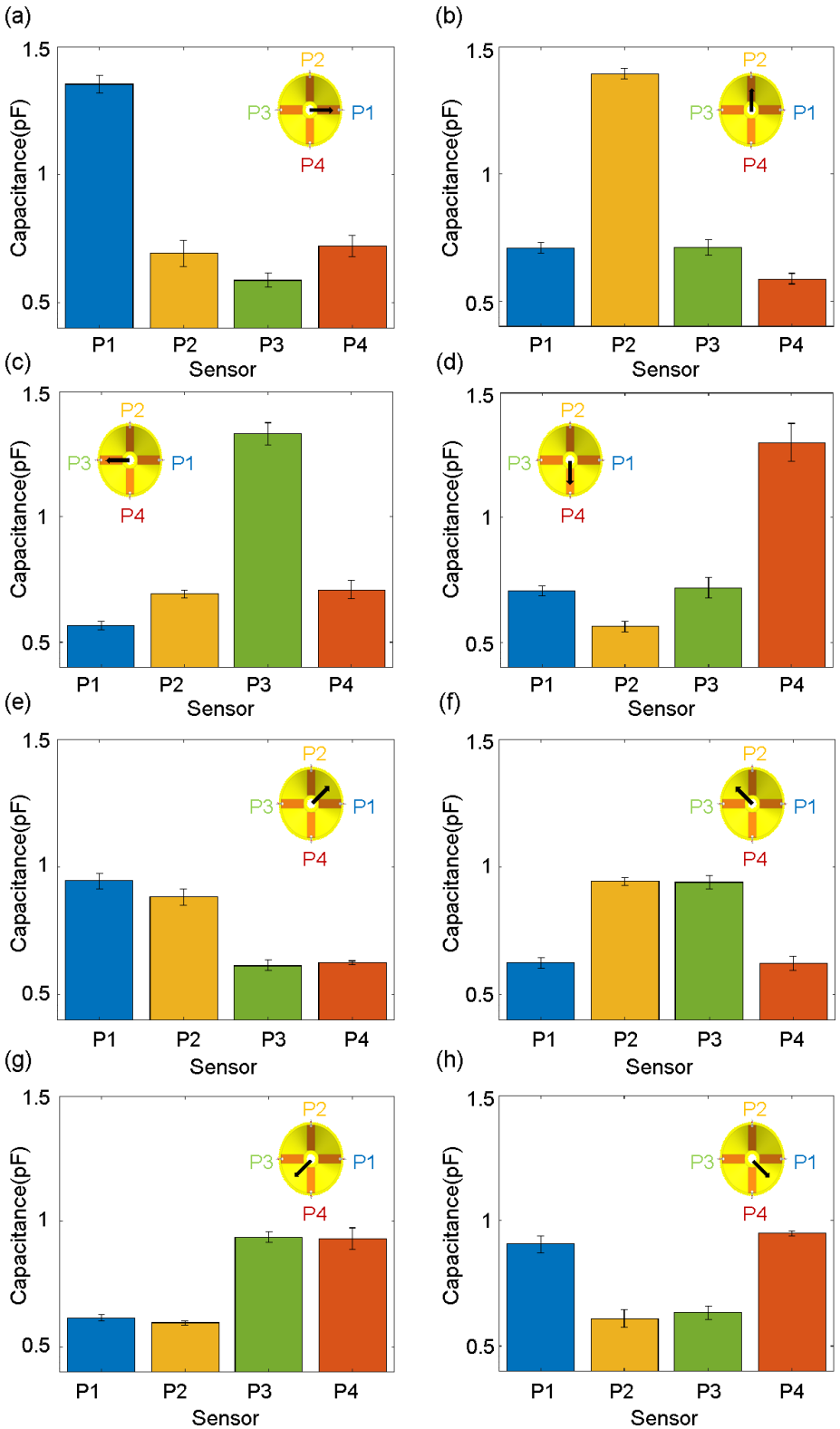

FIGURE 8. Sensing performance of the SCI tilted at 40° along the total eight directions: (a) P1, (b) P2, (c) P3, (d) P4, (e) the intermediate (medial) direction between P1 and P2, (f) between P2 and P3, (g) between P3 and P4, and (h) between P4 and P1.

manufacturing method. When the electrode of the polymer pillar was tilted toward one of the electrode directions of the PLA frame (i.e., P1, P2, P3, and P4 directions), the capacitance between the pillar electrode and the electrode in the tilt direction exhibited the highest capacitance value as the distance between the two electrodes was the smallest,

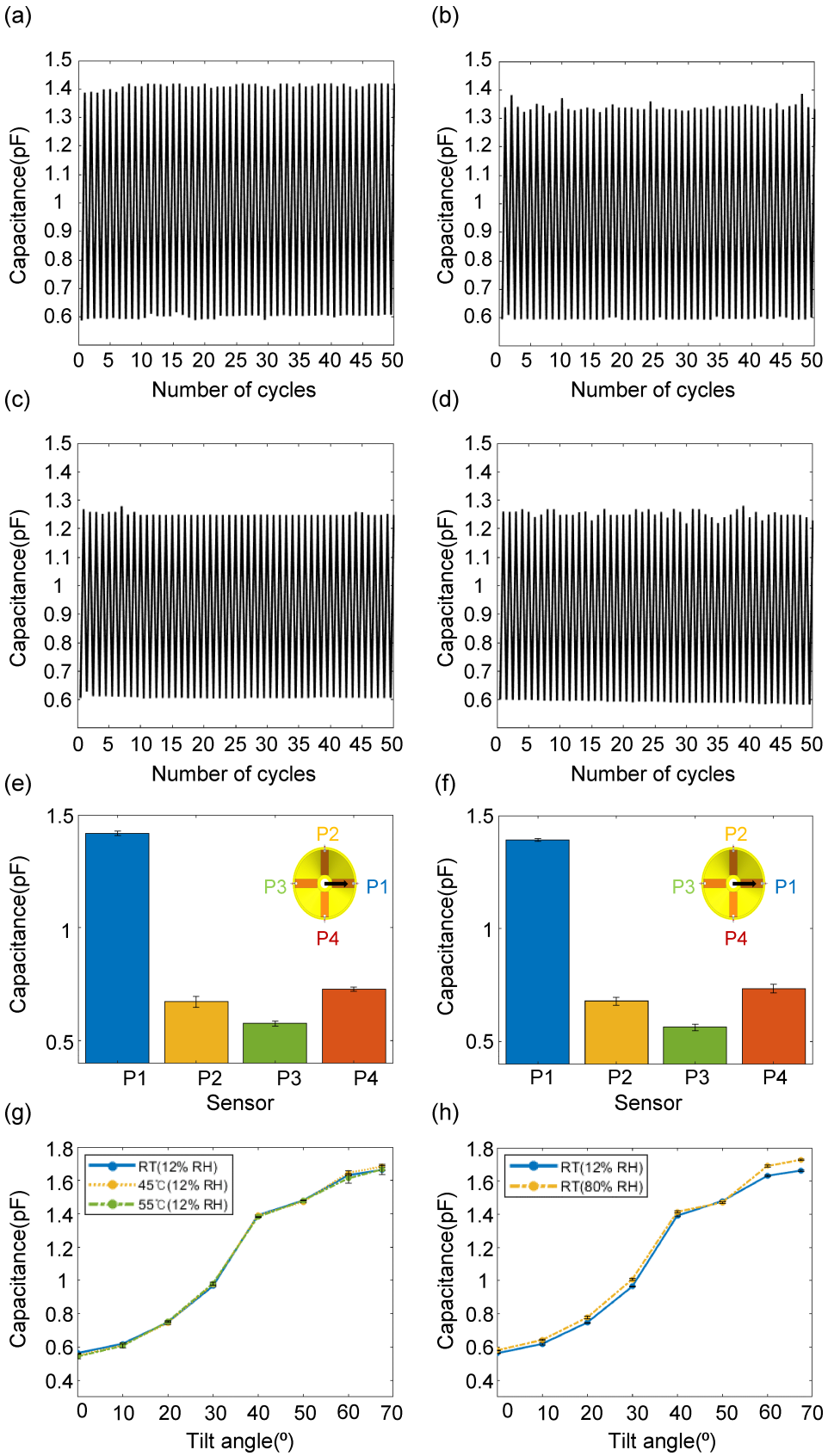

FIGURE 9. The durability test of the SCI. Cycle test at a tilt angle of 40° along the four main directions (50 cycles for each direction): (a) P1, (b) P2, (c) P3, (d) P4. (e) Sensing performance before the cycle test and (f) sensing performance after the cycle test. (g) Capacitance change at different temperatures in P1 direction with fixed RH (12%), and (h) capacitance change at different RHs in P1 direction with fixed temperature (17°C).

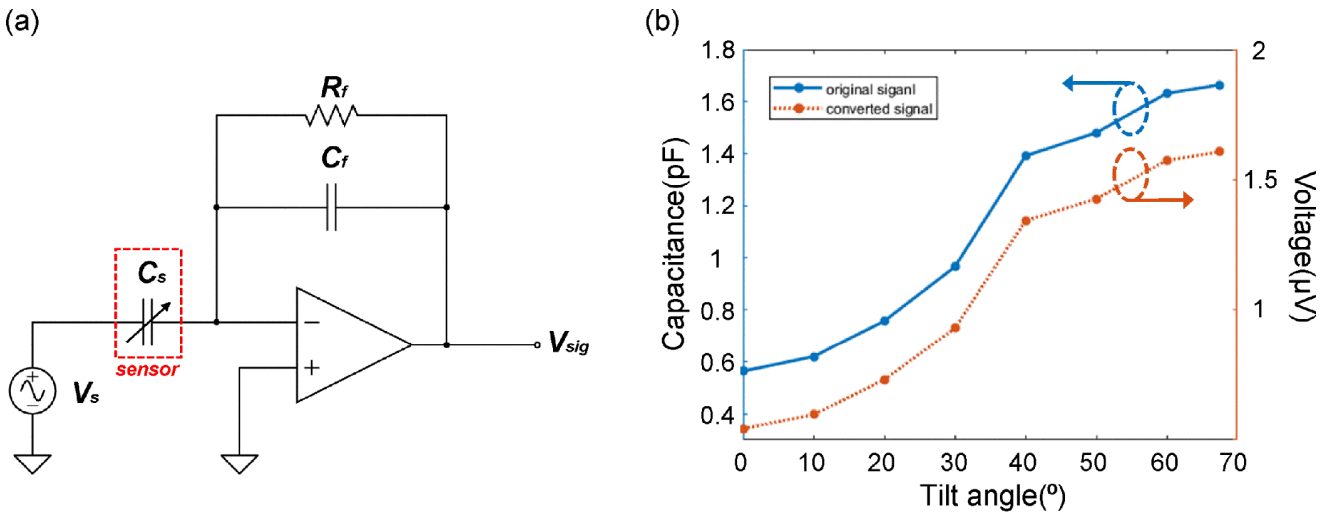

FIGURE 10. (a) Schematic of the basic readout circuit. (b) Converted signal (from capacitance to voltage) by the readout circuit.

as shown in Figs. 8(a), 8(b), 8(c), and 8(d). It should be noted that the capacitance between the pillar electrode and the electrode in the opposite direction to the tilt direction exhibited the lowest value because of the largest distance between the two electrodes (i.e., the P3 electrode for the P1 direction, P4 electrode for the P2 direction, P1 electrode for the P3 direction, and P2 electrode for the P4 direction). In addition, the capacitance between the pillar electrodes and the rest of the electrodes (e.g., P2 and P4 electrodes for the tilt direction of P1) showed similar values as the distance between the pillar electrode and each electrode (P2 and P4) remained similar during the tilting movement. Therefore, in this tilting case, the tilt direction can be easily detected by monitoring one peak capacitance value. When the electrode of the polymer pillar was tilted toward the intermediate (median) direction between adjacent electrodes of the PLA frame, the capacitance of the two electrodes adjacent to the polymer pillar increased at a similar level, whereas the capacitance of the rest of the electrodes in the opposite direction decreased similarly, as shown in Figs. 8(e), 8(f), 8(g), and 8(h).

To characterize the durability and repeatability, the experiments were performed with respect to changes in cycle, temperature, and relative humidity (RH) as shown in Fig. 9. The cycle test was conducted for each 50 cycles along four main directions (i.e., P1, P2, P3, and P4 directions) at the tilt angle from 0° to 40°. As shown in Figs. 9(a)-9(d), there was no significant decrease (degradation) in sensitivity during 50 cycles for each direction. Figures 9(e) and 9(f) show the sensing performance of the SCI with the inclination angle of 40° in P1 direction before and after the cycle test, respectively. As a result, the SCI maintained the constant sensing performance even after cycle test, indicating the repeatability.

To characterize the effect of temperature and humidity on the sensitivity, the SCI was tested under different temperature and humid environments. When the SCI was exposed to room temperature (17°C), 45°C, and 55°C at the fixed RH of 12%, the change in capacitance exhibited no significant difference with respect to the temperature change, as shown in Fig. 9(g). When the SCI was tested under two different RH values (i.e., 12% and 80%) at room temperature, the SCI with 80% RH showed higher value compared to that with 12% RH, as shown in Fig. 9(h). This might be because of an increase in the dielectric constant of air between the pillar and roof frame [51]. Although the sensitivity was slightly affected by the RH, it was confirmed that the temperature and humidity did not significantly affect the sensing performance of the SCI in this study. Therefore, these results reveal that the fabricated SCIs are durable and can be utilized to simultaneously measure the inclination angle and tilt direction.

Figure 10(a) shows the basic concept of the suitable readout circuit for the SCI. The circuit simulation was conducted using LT spice simulator for measuring converted signal from original signal. The capacitance of sensor (C_s) was set to the experiment results with the inclined angle ranging from 0° to 67.5°. The AC voltage source (V_s) was set to sine function, DC offset of 0 V, amplitude of 1 V, and frequency of 60 Hz. C_f and R_f were set to 1 μF and 10 kΩ, respectively. As a result, the aspect of the converted signal was similar to the original signal, as shown in Fig. 10(b). Consequently, the signal conversion from the capacitance of sensor to the voltage output was performed well. With this readout circuit, the SCI may be used with small and portable circuits other than bulky LCR meter. Therefore, the simultaneous measurement, lightweighting, and miniaturization of the measurement system could be further realized.

IV. CONCLUSION

In summary, we demonstrated the facile and cost-effective fabrication of a soft capacitive-type inclinometer that consists of a flexible polymer pillar and PLA roof frame using 3D printing technology to measure both the inclination angle and tilt direction simultaneously. Conventional inclinometers cannot monitor both tilt angles and directions. A comparison of the sensitivities of the two types of polymer pillars used in the SCIs revealed that the performance of the polymer pillar with the electrical connection between the helix copper

electrode and the standard weight was approximately 80% higher than that of the electrically disconnected polymer pillar. By comparing the sensing performance of the three types of PLA roof frames, we found that the SCI with a roof frame angle of 45° exhibited the best sensing performance among all the studied SCIs. In addition, the fabricated SCI could estimate the tilt direction by distinguishing the peak value of the capacitance or comparing the amplitude of the measured capacitance. The durability and repeatability of the SCI were also demonstrated under environmental conditions (i.e., temperature and humidity) and cycle test. By performing the readout circuit simulation using LT spice simulator, the feasibility of development of portable measurement platform with the SCI was demonstrated for further applications. This study supports the use of 3D-printed inclinometers in various industrial applications, such as in drones, submarines, vessels, automobiles, tower cranes, and buildings for structural health monitoring during tilting motions to provide more accurate positions, thus preventing potential disasters.

REFERENCES

[1] S. Wang, Y. Wang, D. Liu, Z. Zhang, W. Li, C. Liu, T. Du, X. Xiao, L. Song, H. Pang, and M. Xu, "A robust and self-powered tilt sensor based on annular liquid-solid interfacing triboelectric nanogenerator for ship attitude sensing," *Sens. Actuators A, Phys.*, vol. 317, Jan. 2021, Art. no. 112459, doi: 10.1016/j.sna.2020.112459.

[2] D. N. Lambert, P. A. Rona, R. H. Bennett, and J. W. Kofoed, "Two inclinometers for the direct measurement of seafloor gradient from a submersible," *Geo-Marine Lett.*, vol. 1, no. 1, pp. 69–72, Mar. 1981, doi: 10.1007/BF02463305.

[3] A. G. Sharp and J. R. Sullivan, "A pendulum inclinometer for use with small deep-submersibles," *Ocean Eng.*, vol. 3, no. 3, pp. 157–158, May 1976, doi: 10.1016/0029-8018(76)90031-7.

[4] K. Rao, H. Liu, X. Wei, W. Wu, C. Hu, J. Fan, J. Liu, and L. Tu, "A high-resolution area-change-based capacitive MEMS tilt sensor," *Sens. Actuators A, Phys.*, vol. 313, Oct. 2020, Art. no. 112191, doi: 10.1016/j.sna.2020.112191.

[5] Y. Chiu, B.-T. Chen, and H.-C. Hong, "Integrated CMOS MEMS liquid capacitive inclinometer," in *Proc. Transducers 18th Int. Conf. Solid-State Sensors, Actuat. Microsyst. (TRANSDUCERS)*, Jun. 2015, pp. 1152–1155, doi: 10.1109/TRANSDUCERS.2015.7181132.

[6] D. Benz, T. Botzelmann, H. Kück, and D. Warkentin, "On low cost inclination sensors made from selectively metallized polymer," *Sens. Actuators A, Phys.*, vols. 123–124, pp. 18–22, Sep. 2005, doi: 10.1016/j.sna.2005.03.044.

[7] I.-S. Kang, H. Jung, C. J. Kim, B. J. Kwon, W.-J. Kim, S.-Y. Choi, J.-H. Lee, J.-K. Shin, and S. H. Kong, "Design and fabrication of a micro electro mechanical systems-based electrolytic tilt sensor," *Jpn. J. Appl. Phys.*, vol. 45, no. 6B, pp. 5626–5630, Jun. 2006, doi: 10.1143/JJAP.45.5626.

[8] F. S. Alves, R. A. Dias, J. M. Cabral, J. Gaspar, and L. A. Rocha, "High-resolution MEMS inclinometer based on pull-in voltage," *J. Microelectromech. Syst.*, vol. 24, no. 4, pp. 931–939, Aug. 2015, doi: 10.1109/JMEMS.2014.2359633.

[9] J. Lu, X. Liu, and H. Zhang, "Tilt measurement using inclinometer based on redundant configuration of MEMS accelerometers," *Meas. Sci. Technol.*, vol. 29, no. 5, May 2018, Art. no. 055004, doi: 10.1088/1361-6501/aaa504.

[10] S. Dalola, V. Ferrari, and D. Marioli, "Micromachined piezoresistive inclinometer with oscillator-based integrated interface circuit and temperature readout," *Meas. Sci. Technol.*, vol. 23, no. 3, Mar. 2012, Art. no. 035107, doi: 10.1088/0957-0233/23/3/035107.

[11] H. Xu, Y. Zhao, K. Zhang, and K. Jiang, "A capacitive MEMS inclinometer sensor with wide dynamic range and improved sensitivity," *Sensors*, vol. 20, no. 13, p. 3711, Jul. 2020, doi: 10.3390/s20133711.

[12] F. Mir and M. Mehran, "Design, analysis and simulation of a novel linear capacitive tilt micro-sensor," *Microsyst. Technol.*, vol. 22, no. 9, pp. 2159–2165, Sep. 2016, doi: 10.1007/s00542-016-3023-z.

[13] J. H. Lee and S. S. Lee, "Electrolytic tilt sensor fabricated by using electroplating process," *Sens. Actuators A, Phys.*, vol. 167, no. 1, pp. 1–7, May 2011, doi: 10.1016/j.sna.2011.01.011.

[14] H. Ueda, H. Ueno, K. Itoigawa, and T. Hattori, "Micro capacitive inclination sensor utilizing dielectric nano-particles," in *Proc. 19th IEEE Int. Conf. Micro Electro Mech. Syst.*, Jan. 2006, pp. 706–709, doi: 10.1109/MEMSYS.2006.1627897.

[15] F. Hosseini, M. Mehran, S. Mohajerzadeh, and O. Shoaei, "Design, analysis, simulation, and fabrication of a novel linear MEMS capacitive inclinometer," *IEEE Sensors J.*, vol. 18, no. 17, pp. 6962–6968, Sep. 2018, doi: 10.1109/JSEN.2018.2851660.

[16] A. B. A. Manaf, K. Nakamura, and Y. Matsumoto, "Characterization of miniaturized one-side-electrode-type fluid-based inclinometer," *Sens. Actuators A, Phys.*, vol. 144, no. 1, pp. 74–82, May 2008, doi: 10.1016/j.sna.2008.01.003.

[17] J. Guo, P. Hu, and J. Tan, "Analysis of a segmented annular coplanar capacitive tilt sensor with increased sensitivity," *Sensors*, vol. 16, no. 1, p. 133, Jan. 2016, doi: 10.3390/s16010133.

[18] L. Järup, "Hazards of heavy metal contamination," *Brit. Med. Bull.*, vol. 68, no. 1, pp. 167–182, Dec. 2003, doi: 10.1093/bmb/ldg032.

[19] T. W. Clarkson, L. Magos, and G. J. Myers, "The toxicology of mercury—Current exposures and clinical manifestations," *New England J. Med.*, vol. 349, no. 18, pp. 1731–1737, Oct. 2003, doi: 10.1056/NEJMra022471.

[20] T. W. Clarkson and L. Magos, "The toxicology of mercury and its chemical compounds," *Crit. Rev. Toxicol.*, vol. 36, no. 8, pp. 609–662, Jan. 2006, doi: 10.1080/10408440600845619.

[21] S. M. Khan, N. Qaiser, and M. M. Hussain, "An inclinometer using movable electrode in a parallel plate capacitive structure," *AIP Adv.*, vol. 9, no. 4, Apr. 2019, Art. no. 045118, doi: 10.1063/1.5092146.

[22] U. Mescheder and S. Majer, "Micromechanical inclinometer," *Sens. Actuators A, Phys.*, vol. 60, nos. 1–3, pp. 134–138, May 1997, doi: 10.1016/S0924-4247(97)01387-3.

[23] R. Puers and S. Reyntjens, "Design and processing experiments of a new miniaturized capacitive triaxial accelerometer," *Sens. Actuators A, Phys.*, vol. 68, nos. 1–3, pp. 324–328, Jun. 1998, doi: 10.1016/S0924-4247(98)00032-6.

[24] M. L. Hoang, M. Carratu, V. Paciello, and A. Pietrosanto, "A new orientation method for inclinometer based on MEMS accelerometer used in industry 4.0," in *Proc. IEEE 18th Int. Conf. Ind. Informat. (INDIN)*, Jul. 2020, pp. 177–181, doi: 10.1109/INDIN45582.2020.9442189.

[25] J. Zhu, W. Wang, S. Huang, and W. Ding, "An improved calibration technique for MEMS accelerometer-based inclinometers," *Sensors*, vol. 20, no. 2, p. 452, Jan. 2020, doi: 10.3390/s20020452.

[26] M. L. Hoang and A. Pietrosanto, "A robust orientation system for inclinometer with full-redundancy in heavy industry," *IEEE Sensors J.*, vol. 21, no. 5, pp. 5853–5860, Mar. 2021, doi: 10.1109/JSEN.2020.3040374.

[27] S.-H. P. Won and F. Golnaraghi, "A triaxial accelerometer calibration method using a mathematical model," *IEEE Trans. Instrum. Meas.*, vol. 59, no. 8, pp. 2144–2153, Sep. 2010, doi: 10.1109/TIM.2009.2031849.

[28] L. Tang, K. Zhang, S. Chen, G. Zhang, and G. Liu, "MEMS inclinometer based on a novel piezoresistor structure," *Microelectron. J.*, vol. 40, no. 1, pp. 78–82, Jan. 2009, doi: 10.1016/j.mejo.2008.06.080.

[29] P. F. C. Antunes, C. A. Marques, H. Varum, and P. S. André, "Biaxial optical accelerometer and high-angle inclinometer with temperature and cross-axis insensitivity," *IEEE Sensors J.*, vol. 12, no. 7, pp. 2399–2406, Jul. 2012, doi: 10.1109/JSEN.2012.2190763.

[30] L.-Y. Shao and J. Albert, "Compact fiber-optic vector inclinometer," *Opt. Lett.*, vol. 35, no. 7, p. 1034, Apr. 2010, doi: 10.1364/OL.35.001034.

[31] O. Frazão, R. Falate, J. L. Fabris, J. L. Santos, L. A. Ferreira, and F. M. Araújo, "Optical inclinometer based on a single long-period fiber grating combined with a fused taper," *Opt. Lett.*, vol. 31, no. 20, p. 2960, Oct. 2006, doi: 10.1364/OL.31.002960.

[32] K. Agarwal, C. Liu, D. Joung, H.-R. Park, S.-H. Oh, and J.-H. Cho, "Three-dimensional anisotropic metamaterials as triaxial optical inclinometers," *Sci. Rep.*, vol. 7, no. 1, p. 2680, Dec. 2017, doi: 10.1038/s41598-017-02865-z.

[33] D.-H. Jeong, S.-S. Yun, B.-G. Lee, M.-L. Lee, C.-A. Choi, and J.-H. Lee, "High-resolution capacitive microinclinometer with oblique comb electrodes using (110) silicon," *J. Microelectromech. Syst.*, vol. 20, no. 6, pp. 1269–1276, Dec. 2011, doi: 10.1109/JMEMS.2011.2167662.

[34] Y. Parmar, N. Gupta, V. Gond, S. S. Lamba, S. R. K. Vanjari, S. Dutta, K. K. Jain, and D. K. Bhattacharya, "Characterization of SOI technology based MEMS differential capacitive accelerometer and its estimation of resolution by near vertical tilt angle measurements," *Microsyst. Technol.*, vol. 26, no. 3, pp. 701–706, Mar. 2020, doi: 10.1007/s00542-019-04561-6.

[35] F. Chen, W. Tian, and Y. Wei, "Highly sensitive resonant sensor using quartz resonator cluster for inclination measurement," *Rev. Sci. Instrum.*, vol. 91, no. 5, May 2020, Art. no. 055005, doi: 10.1063/5.0001406.

[36] E. Esteves Moreira, B. Kuhlmann, F. Serra Alves, R. Alves Dias, J. Cabral, J. Gaspar, and L. A. Rocha, "Highly sensitive MEMS frequency modulated accelerometer with small footprint," *Sens. Actuators A, Phys.*, vol. 307, Jun. 2020, Art. no. 112005, doi: 10.1016/j.sna.2020.112005.

[37] S. Wang, X. Wei, Y. Weng, Y. Zhao, and Z. Jiang, "A novel single-axis MEMS tilt sensor with a high sensitivity in the measurement range from 0° to 360°," *Sensors*, vol. 18, no. 2, p. 346, Jan. 2018, doi: 10.3390/s18020346.

[38] D. D. Shin, C. H. Ahn, Y. Chen, D. L. Christensen, I. B. Flader, and T. W. Kenny, "Environmentally robust differential resonant accelerometer in a wafer-scale encapsulation process," in *Proc. IEEE 30th Int. Conf. Micro Electro Mech. Syst. (MEMS)*, Jan. 2017, pp. 17–20, doi: 10.1109/MEMSYS.2017.7863328.

[39] S.-J. Chen and C.-H. Shen, "A novel two-axis CMOS accelerometer based on thermal convection," *IEEE Trans. Instrum. Meas.*, vol. 57, no. 8, pp. 1572–1577, Aug. 2008, doi: 10.1109/TIM.2008.925347.

[40] B. Kang, J. Hyeon, and H. So, "Facile microfabrication of 3-dimensional (3D) hydrophobic polymer surfaces using 3D printing technology," *Appl. Surf. Sci.*, vol. 499, Jan. 2020, Art. no. 143733, doi: 10.1016/j.apsusc.2019.143733.

[41] B. Kang, J. Sung, and H. So, "Realization of superhydrophobic surfaces based on three-dimensional printing technology," *Int. J. Precis. Eng. Manuf.-Green Technol.*, vol. 8, no. 1, pp. 47–55, Jan. 2021, doi: 10.1007/s40684-019-00163-9.

[42] Y.-Y. Hsu, K. Lucas, D. Davis, B. Elolampi, R. Ghaffari, C. Rafferty, and K. Dowling, "Novel strain relief design for multilayer thin film stretchable interconnects," *IEEE Trans. Electron Devices*, vol. 60, no. 7, pp. 2338–2345, Jul. 2013, doi: 10.1109/TED.2013.2264217.

[43] A. Gallarello, A. Palombi, G. Annio, S. Homer-Vanniasinkam, E. D. Momi, G. Maritati, R. Torii, G. Burriesci, and H. A. Wurdemann, "Patient-specific aortic phantom with tunable compliance," *J. Eng. Sci. Med. Diag. Therapy*, vol. 2, no. 4, pp. 1–12, Nov. 2019, doi: 10.1115/1.4044611.

[44] Y. Zhao, W. Yang, Y. J. Tan, S. Li, X. Zeng, Z. Liu, and B. C.-K. Tee, "Highly conductive 3D metal-rubber composites for stretchable electronic applications," *APL Mater.*, vol. 7, no. 3, Mar. 2019, Art. no. 031508, doi: 10.1063/1.5083942.

[45] R. V. Martinez, J. L. Branch, C. R. Fish, L. Jin, R. F. Shepherd, R. M. D. Nunes, Z. Suo, and G. M. Whitesides, "Robotic tentacles with three-dimensional mobility based on flexible elastomers," *Adv. Mater.*, vol. 25, no. 2, pp. 205–212, Jan. 2013, doi: 10.1002/adma.201203002.

[46] V. Palaniappan, M. Panahi, D. Maddipatla, X. Zhang, S. Masihi, H. R. K. M. Emani, B. B. Narakathu, B. J. Bazuin, and M. Z. Atashbar, "Flexible M-tooth hybrid micro-structure-based capacitive pressure sensor with high sensitivity and wide sensing range," *IEEE Sensors J.*, vol. 21, no. 23, pp. 26261–26268, Dec. 2021, doi: 10.1109/JSEN.2021.3064451.

[47] V. Palaniappan, S. Masihi, M. Panahi, D. Maddipatla, A. K. Bose, X. Zhang, B. B. Narakathu, B. J. Bazuin, and M. Z. Atashbar, "Laser-assisted fabrication of a highly sensitive and flexible micro pyramid-structured pressure sensor for E-skin applications," *IEEE Sensors J.*, vol. 20, no. 14, pp. 7605–7613, Jul. 2020, doi: 10.1109/JSEN.2020.2989146.

[48] S. Ali, D. Maddipatla, B. B. Narakathu, A. A. Chlaihawi, S. Emamian, F. Janabi, B. J. Bazuin, and M. Z. Atashbar, "Flexible capacitive pressure sensor based on PDMS substrate and Ga–In liquid metal," *IEEE Sensors J.*, vol. 19, no. 1, pp. 97–104, Jan. 2019, doi: 10.1109/JSEN.2018.2877929.

[49] S. Masihi, M. Panahi, D. Maddipatla, A. J. Hanson, A. K. Bose, S. Hajian, V. Palaniappan, B. B. Narakathu, B. J. Bazuin, and M. Z. Atashbar, "Highly sensitive porous PDMS-based capacitive pressure sensors fabricated on fabric platform for wearable applications," *ACS Sensors*, vol. 6, no. 3, pp. 938–949, Mar. 2021, doi: 10.1021/acssensors.0c02122.

[50] M. Shavezipur, S. M. Hashemi, P. Nieva, and A. Khajepour, "Development of a triangular-plate MEMS tunable capacitor with linear capacitance–voltage response," *Microelectron. Eng.*, vol. 87, no. 9, pp. 1721–1727, Nov. 2010, doi: 10.1016/j.mee.2009.09.011.

[51] R. Anchisini, G. Faglia, M. C. Gallazzi, G. Sberveglieri, and G. Zerbi, "Polyphosphazene membrane as a very sensitive resistive and capacitive humidity sensor," *Sens. Actuators B, Chem.*, vol. 35, nos. 1–3, pp. 99–102, Sep. 1996, doi: 10.1016/S0925-4005(97)80037-8.

KEUNTAE BAEK received the B.S. degree from Hanyang University, South Korea, in 2021, where he is currently pursuing the M.S. and Ph.D. degrees with the Mechanical Convergence Engineering Department. His research interests include microfabrication of sensors and functional materials for sensing applications.

JOOHYUNG BANG received the B.S. degree from Hanyang University, South Korea, in 2021, where he is currently pursuing the M.S. and Ph.D. degrees with the Mechanical Convergence Engineering Department. His research interests include additive manufacturing, micromachining, and micro/nanosystems.

JIHUN LEE received the B.S. degree from Hanyang University, South Korea, in 2022, where he is currently pursuing the M.S. degree with the Mechanical Convergence Engineering Department. His research interests include biomedical devices, micromachining, sensors, and actuators.

MINYOUNG CHOI received the B.S. degree from Hanyang University, South Korea, in 2022, where she is currently pursuing the M.S. degree with the Mechanical Convergence Engineering Department. Her research interests include micromachining, additive manufacturing, and reactive materials for sensor applications.

HONGYUN SO (Member, IEEE) received the Ph.D. degree in mechanical engineering from the University of California, Berkeley, in 2014. He joined as a Postdoctoral Scholar with the Aeronautics and Astronautics Department, Stanford University, in 2015. He is currently an Assistant Professor with the Mechanical Engineering Department, Hanyang University. His research interests include design, modeling, and manufacturing of micro/nanosystems, harsh-environment sensors, and mechanical issues related to heat transfer and fluid mechanics.